Coastal Engineering 138 (2018) 152–164

Contents lists available at ScienceDirect

Coastal Engineering

journal homepage: www.elsevier.com/locate/coastaleng

Cost-effective erosion monitoring of coastal cliffs

Matthew J. Westoby [a], Michael Lim [b,*], Michelle Hogg [c], Matthew J Pound [a], Lesley Dunlop [a], John Woodward [a]

[a] Department of Geography and Environmental Sciences, Northumbria University, Newcastle upon Tyne, NE1 8ST, UK
[b] Department of Mechanical and Construction Engineering, Northumbria University, Newcastle upon Tyne, NE1 8ST, UK
[c] South Tyneside Council, South Shields, NE33 2RL, UK

ARTICLE INFO

Keywords:
Coastal erosion
Coastal monitoring
Remote sensing
Rock fall
Terrestrial laser scanning
Structure-from-motion (SfM)
Digital surface model (DSM)

ABSTRACT

Structure-from-motion with multi-view stereo (SfM-MVS) methods hold the potential for monitoring and quantifying cliff erosion to levels of accuracy and precision which rival terrestrial laser scanning (TLS) and at a fraction of the cost. We benchmark repeat SfM-MVS against TLS for quantifying rock fall frequency, volume, and cliff face erosion rates for a ~1 km section of coastal cliffs where cliff top infrastructure is threatened by erosion. First, we address a major unknown in these techniques, the number and configuration of control points. Surveys demonstrate that a sparse configuration along the cliff base and top, at spacing equivalent to the cliff height, provides suitable accuracy at acceptable logistic time and expense. Second, we show that SfM-MVS models match equivalent TLS data to within 0.04 m, and that the correlation between intersecting TLS- and SfM-derived rock fall volumes improves markedly above a detection threshold of 0.07 m^3. Rock falls below this size threshold account for ~77.7% of detected rock falls but only 1.9% of the calculated annual eroded volume. Annual erosion rates for the 1 km cliff face as calculated by repeat TLS and SfM differencing are 0.6×10^{-2} m a^{-1} and 0.7×10^{-2} m a^{-1}, respectively. Kilometre-scale patterns of cliff erosion are dominated by localised zones of high-magnitude, episodic failure that are over an order of magnitude greater than background rates. The ability of non-specialist engineers, geologists, geomorphologists and managers to rapidly capture high quality, accurate erosion data in a cost-effective manner through repeat SfM-MVS has significant potential to inform coastal managers and decision makers. To further empower coastal authorities and communities, policy frameworks must be developed to incorporate and interpret these data.

1. Introduction

Significant investment is made into mitigating the risks posed by coastal erosion to buildings, infrastructure, utilities and ecosystems in the coastal zone. For example, an estimated GBP >50 million is invested annually by the UK government to delay coastal erosion in England and Wales (Penning-Rowsell and Pardoe, 2015) whilst annual EU public expenditure on coastline protection during the period 1990 to 2020 from risks posed by coastal flooding and erosion is expected to exceed EUR 5.4 billion (European Commission, 2006). Fundamental to the development of effective coastal management options is a well-developed understanding of rates of coastal erosion, their temporal and spatial distribution, and how these may change under future scenarios of climatic change (Dawson et al., 2009). The challenges of optimising the distribution of funding to combat coastal erosion are further enhanced by widespread policy shifts from holding the existing coastline to a range of managed retreat scenarios (Dickson et al., 2007).

Rates of coastal erosion are used alongside future sea-level rise scenarios as key inputs into predictive models for assessing the coastal erosion risk, often at the regional to national scale (e.g. (Bray and Hooke, 1997; Davidson-Arnott, 2005; Environment Agency, 2009; Hall et al., 2003; Mulder et al., 2011; Nicholls et al., 2013; Pethick, 2001)). Estimated or observed rates of coastal retreat are an internationally recognised severity measure for coastal erosion and are typically used to inform coastal development and management (Roebeling et al., 2013; Pranzini et al., 2015; Lazarus et al., 2016; Thieler and Danforth, 1994a). Specifically, these data form the basis for forecasting future coastal recession, where historic retreat rates are extrapolated in conjunction with models of future sea-level rise, typically using the 'Bruun rule' (Bruun, 1962; Cooper and Pilkey, 2004), to identify areas that are exposed to the greatest erosion risk and inform decisions about future management.

* Corresponding author.
E-mail addresses: mjwestoby@gmail.com (M.J. Westoby), matt.westoby@northumbria.ac.uk (M. Lim).

https://doi.org/10.1016/j.coastaleng.2018.04.008
Received 19 June 2017; Received in revised form 7 February 2018; Accepted 5 April 2018
Available online 8 May 2018

Table 1
Summary of survey methods used to quantify coastal erosion.

Data source or method	Pros	Cons	Example references
Cartographic mapping	Often cover large spatial scales (>10 km). Typically freely available or at low cost.	Subject to mapping inaccuracies which hinder accurate delineation of shoreline or coastline in regions of complex topography. Generally no systematic map production interval. Map resolution often not sufficient for detailed erosion monitoring, i.e. where erosion rates are low.	(Brooks and Spencer, 2010; Dornbusch et al., 2008; Genz et al., 2007; Oyedotun, 2014; Sear et al., 2011; Thieler and Danforth, 1994b)
Aerial photography and photogrammetry	Production of detailed, fine-resolution (≤decimetre) orthoimagery.	Expensive to acquire. Survey interval dictated largely by cost. Requires skill in photogrammetric processing to generate accurate datasets.	(Baily and Nowell, 1996; Costa et al., 2004; Dewez, 2004; Moore, 2000; Moore and Griggs, 2002; Pierre, 2006)
Satellite imagery (optical)	Some products freely available. Can cover large, typically regional, spatial scales.	Freely available imagery is often of coarse resolution (>decimetre). Fine resolution (<decimetre) imagery costly for most coastal monitoring and management projects. Usable imagery hindered by cloud cover.	(Loos and Niemann, 2002; Maiti and Bhattacharya, 2009; Pardo-Pascual et al., 2012; White and El Asmar, 1999)
GPS/GNSS	Permits roving capture of cliff-top or cliff-base topography. Relatively affordable and accurate (typically centimetre - decimetre)	Topographic occlusion can affect signal quality, and thus survey accuracy. Difficult to implement around hazardous cliff environments. Time-consuming to acquire data at spatial density which accurately reflects complex topography.	(Baptista et al., 2011; Feagin et al., 2014; Mills et al., 2005; Montreuil et al., 2013)
Airborne LiDAR	Permits direct topographic reconstruction of extensive coastal stretches (>10 km in a single flight). Some data freely available (e.g. UK Environment Agency), but generally not repeat datasets.	Often prohibitively costly to commission. Monitoring interval primarily determined by cost, also weather conditions. Difficult to resolve near-vertical topography (e.g. cliff faces) in sufficient detail due to sensor viewshed.	(Earlie et al., 2015; Obu et al., 2016; Palaseanu-Lovejoy et al., 2016; Pye and Blott, 2016; Young et al., 2011)
Terrestrial LiDAR	Can generate fine-resolution, precise and spatially continuous topographic data. Permits process-scale erosion analysis.	High purchase and maintenance costs. High power requirements and difficult portability. Survey viewshed limited by system line-of-sight. Some advanced knowledge of topographic differencing methods required to produce spatially distributed erosion maps.	(Feagin et al., 2014; Kuhn and Prüfer, 2014; Lim et al., 2005; Montreuil et al., 2013; Rosser et al., 2005; Rosser et al., 2013)
Structure-from-motion (with multi-view stereo)	Low-cost, requires consumer-grade camera and software purchase. Produces fine resolution and spatially continuous 3D topographic data. Minimal deployment time, suitable for rapid and responsive surveying. Accessible, minimal training required to generate fine-resolution 3D models. UAV-mounted camera can be used to monitor in hazardous areas, and extend areal coverage.	Survey control points necessary for georeferencing and accuracy assessment. Must be manually deployed and surveyed. Some advanced knowledge of topographic differencing methods required to generate spatially distributed erosion maps.	(Brunier et al., 2016; Gibbs et al., 2015; Gienko and Terry, 2014; James and Robson, 2012; Mancini et al., 2013; Lim et al., 2015; Turner et al., 2016; Warrick et al., 2017; Westoby et al., 2012)

Broadly speaking, coastal practitioners are faced with compromising between survey methods for quantifying coastal erosion that either: i) achieve large spatial coverage but that are of coarse resolution or of low quality, or ii) acquire high quality, yet expensive data that are typically highly spatially or temporally constrained. Therefore, a need exists to evaluate emerging survey methods which reconcile cost, accuracy and flexible monitoring frequencies, and that can be implemented at spatial scales which are relevant for informing coastal management. A wide range of methods have been used to monitor coastal erosion processes, and these are summarised in Table 1 along with their key advantages and shortcomings with reference to coastal surveying and erosion monitoring. Briefly, these include: historic cartographic mapping, aerial photography and photogrammetry, satellite imagery, global navigation satellite systems (GNSS), electronic distance meters or total station, airborne and terrestrial laser scanning (ALS, TLS) and, most recently, emergent structure-from-motion with multi-view stereo methods (SfM-MVS). These methods can be subdivided into those which produce 2D planimetric data describing cliff planform and therefore represent a 2D simplification of complex 3D erosion processes (Lim et al., 2010), and those from which spatial variation in the vertical distribution of cliff face erosion can be quantified (e.g. (Rosser et al., 2013; Vann Jones et al., 2015)). Rates of cliff line retreat are commonly spatially and temporally averaged, resulting in crude and potentially inaccurate indications of erosion processes that restrict both management decisions and policy development at the local scale (Moore, 2000).

The last decade or so has seen the increasing deployment of fine-resolution TLS for coastal erosion monitoring (e.g. (Dewez et al., 2013; Gulyaev and Buckeridge, 2004; Lim et al., 2005; Rosser et al., 2005; Rosser et al., 2013; Lague et al., 2013)). TLS can generate accurate, fine-resolution and spatially continuous maps of surface change on high, inaccessible cliff faces. Such datasets have led to significant advances in understanding of cliff erosion processes, including the relative importance of small-scale, progressive failures and low-frequency, high-magnitude changes for controlling cliff face evolution (Collins and Sitar, 2008; Letortu et al., 2015; Lim et al., 2010; Rosser et al., 2007). However, TLS requires skilled operation and processing that typically limits its use for responsive cliff surveys. The costs involved with data collection and processing often result in monitoring programmes of limited periods, frequencies and spatial extents. Surveys are generally concentrated on specific areas of concern (e.g. (Lim et al., 2005; Rosser et al., 2013)) producing detailed, yet localised datasets that may be of limited use for informing wider-scale coastal strategies. To inform management decisions, and to make significant impacts on policy formation, the collection of such high-quality cliff face data needs to be more widely accessible and financially viable.

SfM-MVS photogrammetry uses overlapping image sequences from consumer-grade cameras to generate fine-resolution 3D reconstructions of topography (e.g. (Carrivick et al., 2016; Smith et al., 2015; James and Robson, 2012; Westoby et al., 2012)) and holds significant potential for quantifying spatial and temporal cliff response to environmental forcing. SfM-MVS photosets are increasingly captured using relatively low-cost (<£10,000) and lightweight (<20 kg) unmanned aerial vehicle (UAV or 'drone') systems (e.g. (Casella et al., 2016; Dewez et al., 2016; Drummond et al., 2015; Gonçalves and Henriques, 2015; Harwin and Lucieer, 2012; Mancini et al., 2013; Turner et al., 2016)). Previous studies have benchmarked the performance of terrestrial SfM-MVS

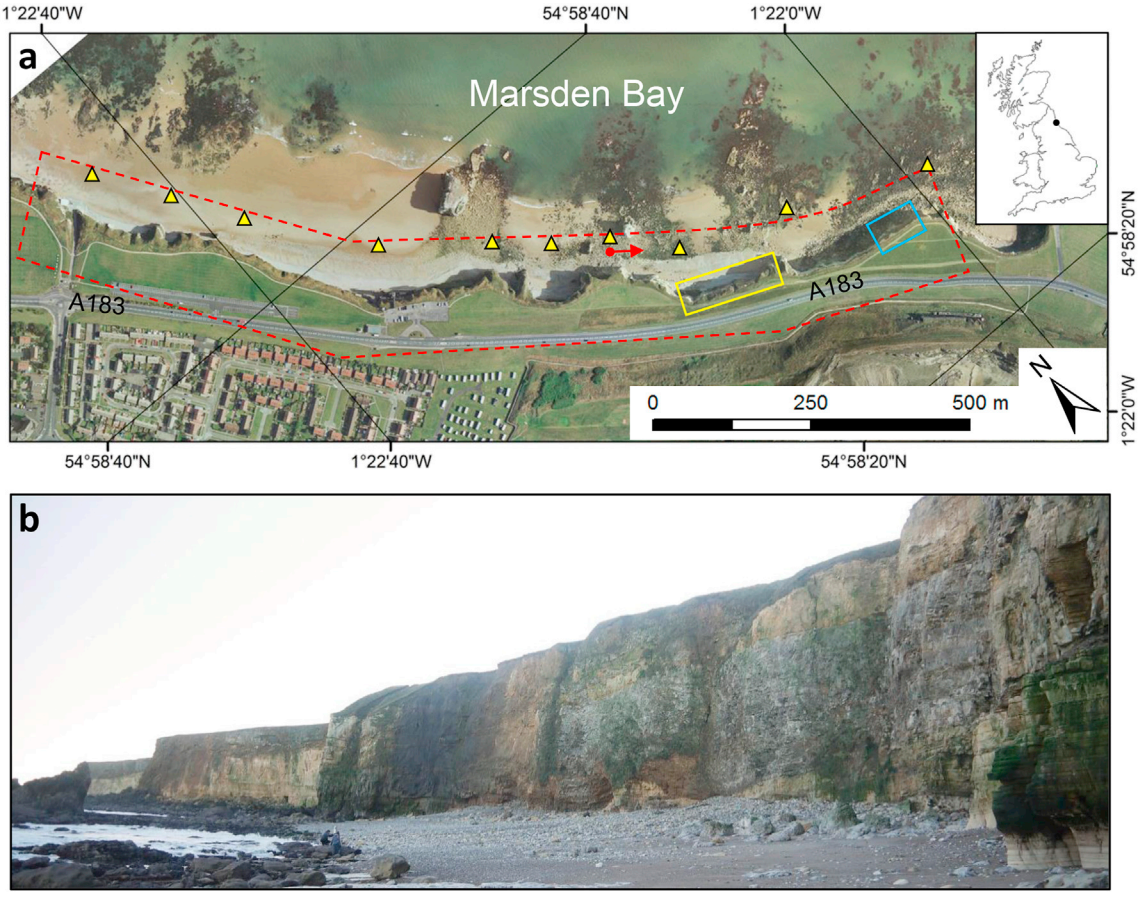

Fig. 1. Study area: a) Site map. Red dashes indicate extent of monitored coastline. Yellow triangles show TLS station positions. Yellow box shows extent of Figs. 2–4. Blue box shows extent of Fig. 6. Red arrow shows camera position and direction for panel b. b) Site photograph, showing hard rock cliff geomorphology. Cliffs are ~25 m in height. Photo: M Westoby. Background to (a) ©DigitalGlobe, extracted from Google Earth. (For interpretation of the references to colour in this figure legend, the reader is referred to the Web version of this article.)

methods against TLS in coastal environments (James and Robson, 2012; Westoby et al., 2012) and have found them capable of generating dense and accurate DEM products that rival those generated from TLS both in terms of data density and accuracy. However, the routine deployment of UAVs typically requires a skilled operator and spotter as a minimum, can be hindered by windy weather conditions typical of rock cliff environments, and is not appropriate at sites where the public may be within the survey area, such as crowded beaches. These restrictions currently reduce the capacity for UAV SfM-MVS surveys to be widely, frequently and responsively implemented for cliff surveys.

The aim of this paper is to evaluate the performance of low-cost, ground-based SfM-MVS photogrammetry for quantifying erosion of a 1.2 km-long section of hard rock coastal cliffs at Marsden Bay, in north-east England. Quantitative comparisons with benchmark TLS data are used to assess and optimise the accuracy and quality of terrestrial SfM-MVS approaches for monitoring cliff face change, primarily through an assessment of the placement of survey control points. The approach has been applied to derive and compare rock fall characteristics (volume, distribution) and cliff face erosion statistics, with a view to presenting terrestrial SfM-MVS as an accessible new tool for non-expert coastal practitioners.

2. Study site

Marsden Bay extends for ~1.6 km along the coastline of north-east England (Fig. 1a). Its north-east orientation exposes it to one of the largest fetch distances on the east coast, exceeding 1900 km. The area is segmented into a series of smaller embayments separated by bedrock promontories. Sporadic, deep-cut caves and discontinuous sections of wave-cut platform occur along the cliff base. The platform areas typically comprise boulder ($>1\ m^3$) fields and pockets of dry pebble and sand beach to the south, with pronounced seepage points exposed at low tide. The cliff face is approximately 25 m in height along its length and is predominantly composed of Permian Magnesian Limestone (Fig. 1b). Structural control, dissolution weathering, and karstic collapse have resulted in layers comprising a variety of geotechnical competencies (ranging from hard to very soft limestone and intact through jointed to brecciated material) becoming exposed within the intertidal zone. This heterogeneity also leads to seepage zones where sporadic ground water flows are concentrated. The tidal range is ~6 m and mean high and low water elevation for the period 21st February 2015 to 26th February 2016 were 2.96 m and −2.25 m above Ordnance Datum Newlyn (mODN), measured at North Shields, 5 km to the north of the study site.

The A183 is an essential road transportation link that joins coastal areas from South Shields to Sunderland (Fig. 1a). In places, the road passes within 15 m of the present cliff edge, resulting in three 'pinch point' areas of concern for the medium term (25 year) viability of the road. Here we focus on a ~1 km section of the wider bay frontage (Fig. 1a). The cliffs are thought to have remained stable over the last 100 years from historic cliff line analysis, despite a predicted future retreat rate of $0.2\ m\ yr^{-1}$ (Environment Agency, 2009). To aid key decisions regarding the management of the road, new quantitative data are required to better discern the rates and nature of coastal cliff retreat at the pinch points.

3. Ground-based SfM-MVS for erosion monitoring

This study compares ground-based photographs processed with SfM-MVS against repeat TLS at Marsden Bay. The following sections describe data acquisition, post-processing and filtering, and the extraction of rock fall and erosion rate statistics.

3.1. Field data collection

Coincident TLS and SfM cliff face surveys were conducted on 21 February 2015 and 26 February 2016. TLS surveys were acquired using a Riegl LMS-Z620 time-of-flight terrestrial laser scanner, set to acquire ~11,000 points per second at a 3D point spacing of 0.05 m at 100 m distance. TLS data acquisition settings were consistent for both surveys. For each survey date, we acquired scans of the cliff face from ten positions with overlapping viewsheds (Fig. 1). TLS field data collection took ~5 h to complete, including station setup, scanning, and transport to successive station positions. TLS scans were manually edited in Riegl RiSCAN PRO software (v. 1.5.9) to remove erroneous 3D point outliers (e.g. seabirds in flight, solar glare) and any visible areas of the foreshore, which were not the focus of our investigation. Overlapping scans acquired on the same survey date were aligned using an iterative closest point (ICP) algorithm in RiSCAN PRO to produce a single 3D point cloud that was scaled and oriented correctly in 3D space. Total station data acquired in 2015 were used to assign real-world elevations (metres above Ordnance Datum Newlyn) to the surface models.

For the SfM-MVS component of the field data collection original resolution (3456 × 2592 px) photographs of cliffs at the site were acquired from the shoreline using a 14.7 MP Canon PowerShot G10 digital camera (sensor size 7.44 × 5.58 mm), with automatic exposure and focusing settings enabled. A total of 405 and 432 photographs of the cliff face were acquired in 2015 and 2016, respectively. The distance between the camera and the base of the cliff was simply set to maximise the cliff face within the viewfinder; this distance ranged from ~25 to 30 m. The optical axis of the camera was perpendicular to the cliff plane, and camera-camera baselines, or the distance between successive photographs, were approximately 2 m. Photoset acquisition for the study area took 2.5 h and 2.0 h for the 2015 and 2016 surveys, respectively, by a non-expert operator with general instruction on the principles of SfM-MVS photograph collection, namely that each successive photo should look very similar but slightly offset from the previous taken. The horizontal overlap between successive photographs was approximately 90% for both SfM-MVS surveys.

Existing studies (James and Robson, 2014) advocate the acquisition of SfM-MVS photographs oriented both obliquely and normally to the target surface to counter against the introduction of model surface deformations, often manifested as a 'doming' effect. Here, we deliberately adopt the simplest form of photograph acquisition to reduce both the time taken to acquire input photographs in the field and also the computational burden associated with increasing the size of the input photoset. We note that the use of a well-distributed network of ground control points (GCP) has been demonstrated to reduce the degree of systematic model deformation where oblique imagery is unavailable (James and Robson, 2014), although residual errors may remain.

3.2. SfM-MVS model generation

The photograph sequences were input into Agisoft PhotoScan Professional Edition (v. 1.2.3) software (Agisoft, 2016) for SfM-MVS reconstruction. PhotoScan employs a proprietary SfM-MVS workflow to reconstruct 3D scene geometry, which includes the identification and matching of unique image tie-points across input photographs followed by an iterative bundle adjustment to solve for internal and external camera orientation parameters. The software enables the user to specify a camera lens distortion model if one is available, however, for simplicity, we permitted the software to undertake self-calibrating bundle adjustment to estimate the camera lens distortion model. Following camera alignment and sparse point cloud reconstruction, only points that were matched in 3 or more photographs and had a reprojection error <0.5 pixels were retained. GCP data were extracted from the coincidentally acquired TLS scan data and were used to optimise the camera alignment and scale and transform the point-cloud, although these data could be substituted with *xyz* GCP positions acquired using a total station. To account for spatial discrepancies between the position of known features in the TLS data, which appear as 3D points, and their equivalent appearance and manual identification in the SfM-MVS photographs, we assigned a spatial 'marker accuracy' (more correctly a measure of marker

placement precision) of 0.05 m during the PhotoScan referencing process. This spacing is approximately double the 3D point spacing of the TLS data, and, following visual inspection, was deemed an appropriate tolerance within which to allow the software to scale and orient the models. Further information on GCP placement and model alignment are described in the following section.

3.3. SfM-MVS model optimisation for cliff erosion monitoring

Previous research has highlighted the sensitivity of SfM-MVS model accuracy to the number and distribution of GCPs (e.g. (James and Robson, 2012; James et al., 2017a)). However, uncertainty and a lack of guidance surround the number and spatial distribution of GCPs required to adequately refine the estimated camera positions and parameters for coastal cliff environments (Ružić et al., 2014). PhotoScan permits software-guided placement of GCP marker positions based on an underlying mesh, although the necessary manual checking and refinement of GCP positions remains a time-consuming process. Depending on the number of GCPs requiring placement and refinement, this can be the longest stage in the SfM-MVS workflow and require the most user interaction. Here we evaluate the evolution of model accuracy resulting from varying the number and distribution of GCPs across the face of an eroding sea cliff, with a view to identifying an optimum arrangement that balances model accuracy improvements whilst minimising the required labour invested.

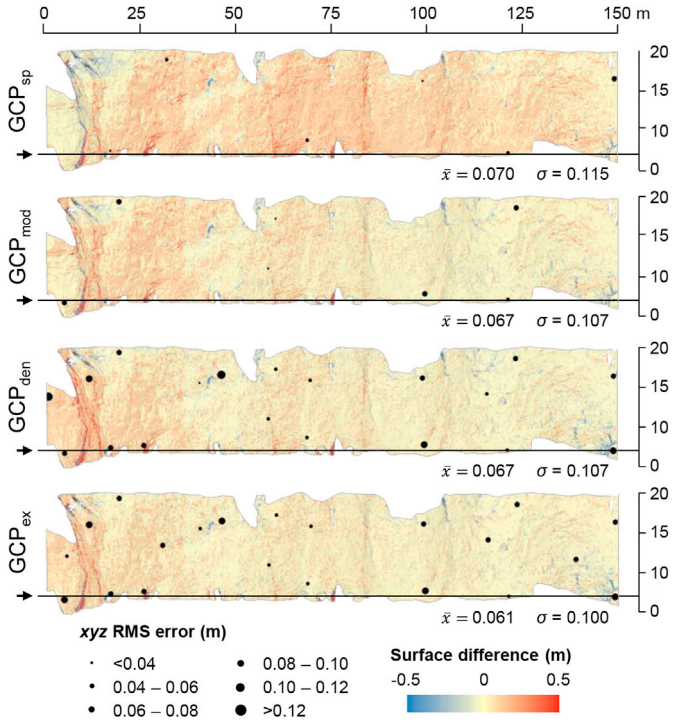

Fig. 2. Comparison between TLS- and SfM-derived surfaces from the February 2015 survey. Each panel is a difference map produced by subtracting the SfM-derived surface from a TLS-derived surface, which is identical in each case. Black dots indicate GCP locations and are scaled according to the magnitude of xyz RMS alignment error. Vertical scale is metres above Ordnance Datum Newlyn (mODN). Black arrow indicates highest astronomical tide (including surges, but excluding wave setup) during the monitoring period from North Shields, 5 km north of the study site. $\bar{x}$ and σ are mean surface difference (m) and standard deviation (m), respectively.

The influence of four GCP placement scenarios on cliff surface form and annual cliff change detection capabilities have been evaluated against coincident TLS surveys for a 150 m-long sub-section of the study area (Fig. 2). These range from a sparse GCP distribution, where GCPs are alternately placed along the cliff top and cliff base (GCP_{sp}), through progressive increases in control for moderate (GCP_{mod}) and dense (GCP_{den}) scenarios, to an extremely dense configuration including systematic placement along the cliff top and base, with additional GCPs in the centre of the cliff (GCP_{ex}).

Following GCP placement and initial 3D transformation in PhotoScan (described in section 3.2) the SfM-MVS point clouds were imported into RiSCAN Pro software, where the alignment between the 2015 and 2016 SfM-MVS point clouds for each GCP configuration was improved using ICP adjustment in the same manner as described previously for the TLS data. Residual alignment errors between successive TLS and SfM-MVS point clouds are shown in Table 2. For methodological consistency, we apply this same final alignment step to the dense point clouds produced using both methods. The aligned TLS and SfM-MVS point cloud data were surfaced in Quick Terrain Modeller software (v.8.0.3.4) to produce a 0.10 m-resolution digital surface model (DSM) for each survey date. Cliff face DSMs were imported into ESRI® ArcMap™ (v. 10) to extract surface change. DSMs from successive surveys were differenced to generate a digital elevation model of difference (DoD), which is an established geomorphological technique for quantifying surface change in a range of environments (e.g. (Abellán et al., 2014; Williams et al., 2012)).

Inspection of the positional errors for individual GCPs within the SfM-MVS reconstructions show these to be generally sub-decimetre (Fig. 2), in line with the findings of previous studies in rocky coastal environments (Ružić et al., 2014). Notably higher residuals are found at the southern end of GCP_{mod} and GCP_{den} DoDs (between 0 and 10 m). An initial comparison between TLS- and SfM-derived surface models for a 150 m-long representative section of the February 2015 survey reveals that the alignment and surface deviation between the two surface gradually improves as the number of GCPs used for SfM model alignment increases; the mean distance and standard deviation decreases from 0.070 ± 0.115 m for GCP_{sp} to 0.061 m ± 0.100 for GCP_{ex}. Areas with the highest residual errors are found toward the south of the sub-section and corresponds with the location of a rock buttress. In all cases, >80% of TLS-SfM surface deviations are within ±0.10 m, increasing from 82% for GCP_{sp} to 86% for GCP_{ex}. Similarly, deviations ±0.05 m cover a minimum of 52% to a maximum of 58% of the surface and increase with GCP densification.

Comparisons between SfM and TLS DoDs are shown in Figs. 3 and 4. Background surface deviations in the TLS DoD appear to be relatively uniform, in contrast with the apparent systematic under- or over-estimations derived from the SfM-MVS data (James and Robson, 2014). For instance, we observe a mean surface difference of ~0.15 m between 100 m and 125 m distance in the GCP_{sp} DoD in an area which, based on the TLS DoD, we expect to record no surface change. Similarly, we observe negative surface differences of a similar magnitude between 95 m and 105 m in GCP_{den}, which are reduced in GCP_{mod} to 0.10 m. Such

Table 2
Summary registration error and change detection statistics for different GCP configurations.

	RMS error (m)	Mean surface difference (m)	Eroded vol. (m3)	No. changes detected	% intersect TLS-TLS
TLS – TLS	0.015	-0.019 ± 0.154	36.47	442	
GCP_{sp} – GCP_{sp}	0.029	0.016 ± 0.330	37.28	306	63.1
GCP_{mod} – GCP_{mod}	0.029	-0.038 ± 0.036	39.38	761	77.7
GCP_{den} – GCP_{den}	0.026	-0.050 ± 0.321	42.03	707	81.9
GCP_{ex} – GCP_{ex}	0.025	-0.033 ± 0.334	52.46	719	78.9

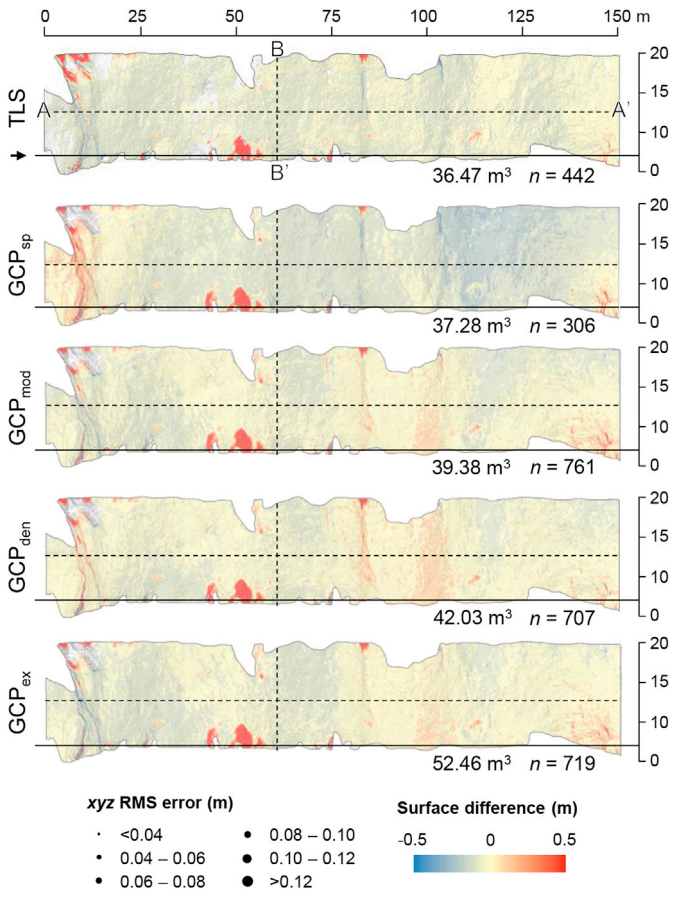

Fig. 3. GCP number and placement: effects on change detection. Panels show raw differencing results for TLS differencing and four GCP placement scenarios. Vertical scaling shows height above sea level (mODN). Black arrow indicates highest astronomical tide (including surges, but excluding wave setup) during the monitoring period from North Shields, 5 km north of the study site. The total erosion volume and number of failure events are shown to the bottom-right of each panel. Profiles A and B relate to Fig. 4 and 5, respectively.

oscillating surface deformations in SfM-MVS-derived models of coastal cliffs are consistent with the findings of James and Robson (2014), who advocate the coincident collection of convergent imagery, or adjustment of the radial distortion parameter, K_1, to mitigate against the introduction of systematic model errors, which we do not explore here.

The standard deviation of surface differences between equivalent TLS and SfM models provides an initial indication as to the magnitude of the variability in form between the two static surfaces. Our analysis reveals a decrease from ±0.191 m (GCP_{sp}) to ±0.163 m (GCP_{mod}) with initial GCP densification. Thereafter, the addition of further GCPs does not reduce this metric significantly; ±0.165 m and ±0.159 m for GCP_{den} and GCP_{ex}, respectively. Fig. 3 illustrates improvements in SfM-MVS DoD quality gained through initial GCP densification; most notably a reduction in the amplitude of DoD convergence error (base level of difference, assumes that the majority of the surface has not changed significantly between surveys). The standard deviation of surface difference across the subsection decreases between GCP_{sp} to GCP_{mod} from ±0.330 m to ±0.036 m (Table 2). The addition of further GCPs does not reduce the DoD standard deviation significantly; ±0.321 m and ±0.334 m for GCP_{den} and GCP_{ex}, respectively, although qualitatively it appears that the magnitude of negative and positive surface deformations decrease with GCP network densification (Figs. 3 and 4). Vertical cliff face profiles highlight a marked improvement in relative SfM-MVS and TLS DoD agreement when GCPs are added to the top and base of the cliff (GCP_{mod}) (Fig. 5). These results appear to imply that improvements in model accuracy can be gained using increasingly dense GCP distributions, but that gains can be marginal beyond a moderate configuration that comprises GCPs placed at the top and base of the cliff and at a spacing which approximates the cliff height. This finding is consistent with existing studies (e.g. James et al., 2017a) which identify a general insensitivity to model quality when the number of GCPs is increased beyond a given threshold.

3.4. Topographic differencing for quantifying cliff face erosion

A more applied assessment of DoD performance for the application of erosion monitoring is the extraction and comparison of individual erosion scars and their associated volumes (Fig. 6). The following processing steps were applied to both SfM-MVS and TLS DoDs to develop a final dataset of spatially distributed cliff face erosion: i) removal of instances of surface loss with depths <0.10 m, in line with change detection thresholds used in similar coastal erosion studies (Rosser et al., 2005); ii) multiplication of the mean depth of retained failures (m) by their surface area (m^2) to calculate eroded volume (m^3); iii) manual removal of errors associated with topographic occlusion; iv) application of a slope filter to remove detected losses intersecting abrupt breaks of slope, where alignment errors can be magnified; v) removal of losses associated with vegetation dieback and seabird nesting activity (identified using corresponding SfM orthoimages); and vi) removal of changes where the failure depth exceeded failure width, in accordance with the geometric properties of observed rock fall scars at the site. Minimum detected failure volumes were 1.0×10^{-3} m^3. Erosion data have been clipped to a common spatial extent to account for slight variations in TLS viewshed between successive surveys.

The comparison of annual volumetric loss across the cliff face subsection reveals a general agreement between the TLS DoD (36.47 m^3) and those corresponding to GCP_{sp} and GCP_{mod} (Fig. 7a); 37.29 m^3 and 39.38 m^3, equating to a volumetric difference of 2.2% and 7.8% respectively (Fig. 6a). Total eroded volumes established using GCP_{den} and GCP_{ex} are higher, and represent percentage increases in volumetric loss of 14.1% and 38.0%, respectively. We find complex variation in key percentiles for rockfall volume distributions between GCP scenarios (Fig. 7b); median rockfall volumes are 0.004 m^3, 0.002 m^3, 0.003 m^3 and 0.003 m^3 for GCP_{sp} – GCP_{ex}, respectively, whilst respective 95th percentiles are 0.091 m^3, 0.018 m^3, 0.044 m^3 and 0.025 m^3. Further, despite the substantial relative overestimation of total eroded volume, we find that the percentage contribution of different rockfall size fractions using GCP_{ex} most closely mirrors that of the TLS-derived rockfall inventory, followed by GCP_{mod} (Table 3). The largest difference in percentage contributions are attributable to GCP_{sp} and GCP_{den}, particularly for rockfalls >1 m^3. There were no significant differences between the rock fall magnitude-frequency relationships derived from TLS differencing and each GCP placement scenario; the power law exponent was found to vary <0.1 (Fig. 7c). The similarity exhibited by the magnitude-frequency relationships despite notable differences in total eroded volume implies that additional rock falls are detected across the full size-distribution as the GCP network increases in density, although the contribution of these fractions relative to the TLS data vary (Table 3).

In our workflow, the total time required for georegistration of a coastal cliff increases approximately linearly with the number of GCPs (or 'markers' in PhotoScan). For instance, in the GCP_{sp} test case, six GCPs were projected (and required reviewing) a total of 348 times across 181 photographs. Assuming a user-guided positional refinement time of 10s per marker, this equates to a total time of 0.97 h. In contrast, GCP_{ex} required the placement and review of 26 markers, which were projected a total of 1190 times across the same 181 photographs. This equates to a total marker refinement time of 3.31 h for the same 150 m-long section of coast. Applying this difference of ~2.3 h per 150 m to the full 1.6 km length of Marsden Bay creates an additional 14.6 h of user input (total 10.7 h and 25.3 h for refinement of 6 and 26 marker configurations, respectively). Our results imply that this additional time investment may

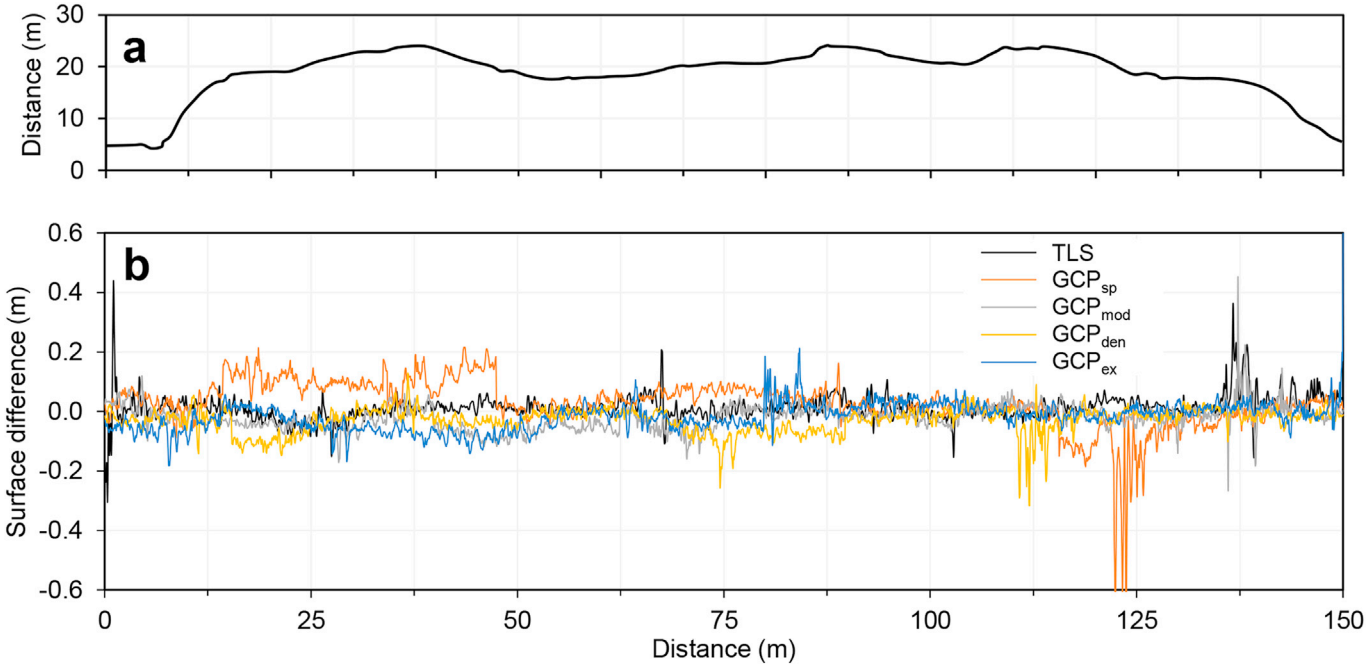

Fig. 4. Comparison of SfM- and TLS-derived cliff surface profiles. a) Cross-shore topographic profile of the cliff face, extracted from the TLS data, where the y-axis shows landward distance. b) Surface difference along a 150 m-long profile through the centre of the cliff face. These data reflect profiles extracted from the TLS-TLS and four SfM-SfM DoDs. Isolated large (~0.5 m) surface differences are the product of model misalignment on breaks of slope, manifested as amplified surface change. See Fig. 3 for profile location.

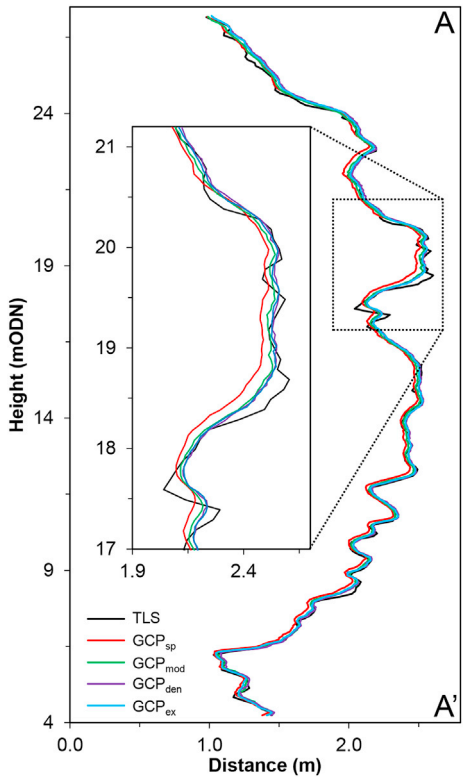

Fig. 5. Vertical profile through cliff face surface models created using TLS and SfM-MVS data acquired in February 2016. SfM-MVS data represent four GCP distributions applied to an identical photoset. These GCP distributions are shown in Fig. 2. See Fig. 3 for profile location.

not produce an appreciable improvement in reconstruction accuracy. Altering additional processing settings in PhotoScan, such as the 'quality' of camera alignment, and dense point cloud generation, will additionally increase or decrease the total SfM-MVS processing time, but are not considered here. Considering these findings, the GCP distribution used in construction of the GCP_{mod} model was considered optimal for balancing acceptable DoD accuracies and total volumetric losses relative to the TLS differencing results, along with an effective and efficient overall processing burden. This GCP configuration was applied for SfM-MVS model generation across the wider study area.

3.5. Analysis and refinement of SfM-derived erosion volumes

The overall eroded volume across the wider study area is 164.77 m^3 and 199.29 m^3 for TLS and SfM-MVS differencing, respectively. TLS differencing produces a higher relative contribution of rock falls $<0.02\ m^3$ relative to the SfM differencing data, whilst the frequency of rock falls $>0.02\ m^3$ is typically higher for the results of SfM differencing (Fig. 8a). Mean and median volumes for intersecting TLS- and SfM-derived rock falls show a close agreement (Fig. 8b), whilst comparison of the spatially averaged erosion rate of the cliff face shows a deviation of 0.001 m a^{-1}, which is negligible over the monitoring interval. Analysis of the relationship between individual intersecting TLS and the filtered SfM-MVS derived rock fall volumes (Fig. 9) reveals considerable mismatch for smaller ($<0.07\ m^3$) rock falls, whilst above this size threshold the variance with TLS reduces. Notable outliers exist above this size threshold where SfM-derived rock falls possess larger volumes than their TLS-derived counterparts. Following further visual inspection of the differencing data, these outliers are attributed to the incomplete reconstruction of these rock falls in the TLS data, primarily due to topographic occlusion. However, it remains unclear whether the increased frequency of the smallest rock fall size fractions reflect genuine change, which is undetected by TLS, or is artificial, and must therefore be removed to arrive at a robust estimate of genuine surface loss.

In contrast, the SfM data are less prone to this effect at larger rock fall volumes due to the roving nature of input photograph collection, and hence tend to produce more spatially complete topographic models and accurately capture pre- and post-rock fall cliff geometries. Whilst intersecting rock falls $>0.07\ m^3$ account for 25.9% and 22.3% of the total rock

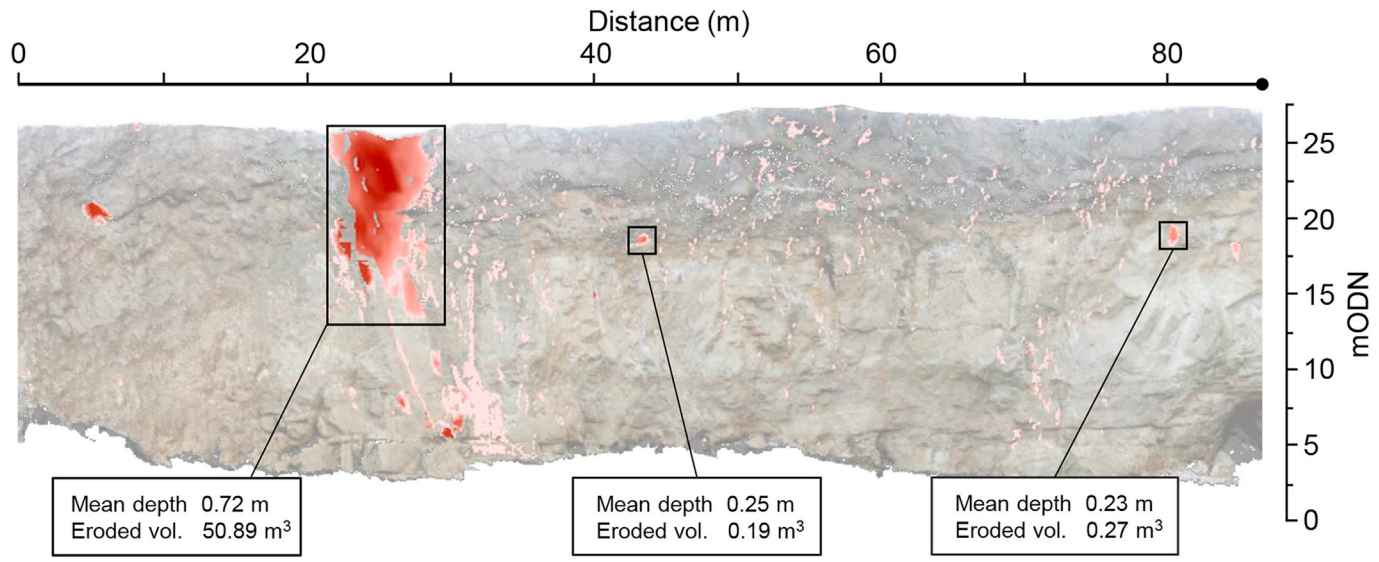

Fig. 6. Example of filtered cliff face erosion data from SfM-SfM differencing. Notable erosion scars and their key descriptors are highlighted for reference. See Fig. 1 for location. Background image is a semi-transparent, SfM-derived orthophoto.

fall count for the SfM and TLS datasets, respectively, they account for 97.5% and 98.1% of total surface erosion. This observation explains why we observe a larger overall eroded volume from SfM-MVS differencing relative to the results of TLS differencing. Removing rock falls $<0.07\ m^3$, which corresponds to material dimensions of $0.41\ m \times 0.41 \times 0.41\ m$, reduces total eroded volume but results in a strong correlation (Pearson correlation = 0.98) between the two datasets. Total eroded volumes for intersecting rock falls $>0.07\ m^3$ were $117.63\ m^3$ and $125.71\ m^3$ for TLS and SfM datasets, respectively. Based on these results, only rock falls $\geq 0.07\ m^3$ have been retained for wider spatial analysis of cliff face erosion rates (Fig. 10).

3.6. Kilometre-scale patterns of cliff erosion

Volumetrically thresholded rock fall data have been amalgamated into 5 m-wide cliffline distance bins and divided by the equivalent cliff face area to derive a spatially distributed model of annual cliff face erosion, which are presentable in a format which is straightforward to interpret by coastal managers (Fig. 10). Spatial analyses of TLS- and SfM-MVS-derived patterns of face retreat reveal a general agreement between the two datasets. The mean rate of cliff face recession along the study area is $0.6 \times 10^{-2}\ m\ a^{-1}$ for TLS differencing, and $0.7 \times 10^{-2}\ m\ a^{-1}$ for SfM-MVS differencing. However, we note that this rate is based on a single year's worth of monitoring data, and may not in fact be representative of medium- and long-term erosion rate trends, which would become better constrained through the acquisition and differencing of multi-year topographic datasets. Both datasets identify areas of locally enhanced retreat, which are attributable to large individual rock falls or progressive failures. Notable examples include measured face retreat of $\sim 0.2\ m\ a^{-1}$ at 0.85 km distance, corresponding to a $\sim 16.7\ m^3$ erosion scar, as well as a zone of particularly high erosion ($\sim 0.6\ m\ a^{-1}$) at ~ 1.0 km distance resulting from surface loss that exceeds $50\ m^3$ in both datasets (Fig. 6). Both examples exceed the site-wide mean by over an order of magnitude. Patterns of rock fall activity imply failure attributable to direct wave action, such as the occurrence of sizeable ($3–4\ m^3$) erosion scars at the base of the cliff (e.g. Fig. 3). The presence of erosion scars at locations close to, or adjacent to the cliff top boundary, where groundwater seepage and surface runoff has been observed in the field, provide some insight into the potential role of precipitation as a driver of cliff face instability.

4. Discussion

4.1. A comparative analysis of terrestrial SfM-MVS with TLS for cliff erosion monitoring

Here we demonstrate that terrestrial photography processed with SfM-MVS methods is appropriate for the 3D reconstruction of hard rock coastal cliff topography. The placement of GCP markers along the top and base of a ~25 m-high cliff at a horizontal spacing which approximately correlates with the cliff height is sufficient and effective for producing high quality SfM-MVS models. Our results suggest that ensuring a quasi-uniform spacing of GCPs along the periphery of the survey area provides adequate control with which to improve model accuracy, which is in line with best practice from the existing literature (e.g. (Carrivick et al., 2016; James et al., 2017b; Smith et al., 2015)). In contrast, adopting a sparse GCP configuration that alternates along the top and base of the cliff in a 'zig-zag' pattern (GCP_{sp}) degrades model quality and enhances surface noise. When aligned and differenced from subsequent models of the same area, cliff face change can be detected (Figs. 3 and 6). This approach appears to generate the potential for more changes to be detected relative to those established with TLS surveys, the current industry standard for erosion monitoring. Therefore, we employ volumetric filtering to remove change above a detection threshold to produce erosion statistics that closely mirror those attainable using TLS differencing (Figs. 9 and 10). Future developments in the field of direct georeferencing, which largely negate the requirement for GCP networks, are anticipated to produce significant gains in the SfM-MVS workflow, although they currently remain in their infancy (e.g. (Carbonneau and Dietrich, 2016; James et al., 2017b)).

Additional rock falls detected in GCP_{den} and GCP_{ex} were mostly concentrated on cliff faces oblique to the TLS during data acquisition. In such areas, we might expect the quality of TLS laser returns to degrade and the point density to decrease, which in turn would decrease the accuracy of surface reconstruction and potentially lead to genuine rock falls being missed. This would lend support to the theory that the additional eroded volume produced by using a denser SfM-MVS GCP network is genuine, since camera network geometry largely mirrors the cliff planform, producing a more uniformly distributed point cloud geometry on oblique faces (and those which appear oblique in the TLS data). A similar effect was noted by James and Robson (2012), who observed that

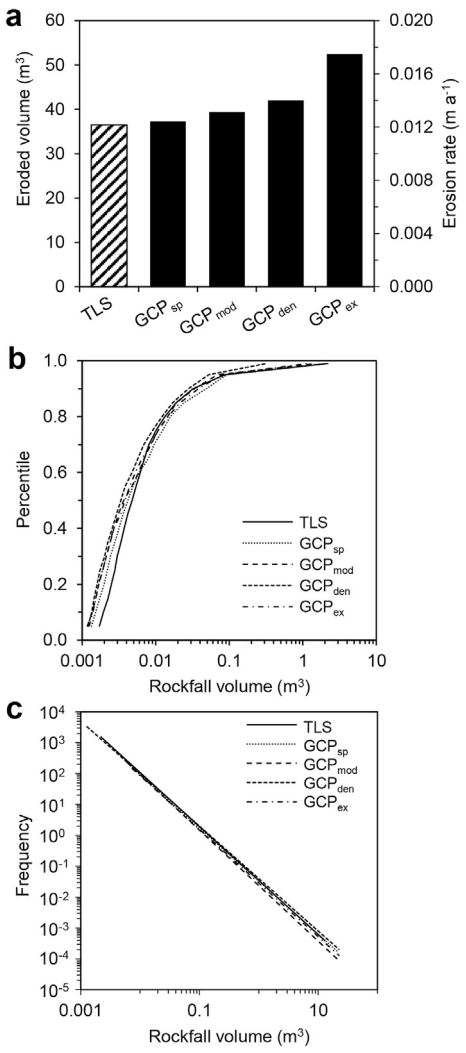

Fig. 7. a) The evolution of volumetric loss and cliff face erosion rate as extracted from differencing of repeat TLS and repeat SfM-MVS models for a 150 m-long sub-section of the study site. The SfM-MVS data comprise models incorporating an increasing density of ground control points (GCP_{sp} – GCP_{ex}). b) percentile contribution of rockfall volumes for different GCP configurations. c) magnitude-frequency relationships for rock falls extracted from TLS-TLS differencing and the four SfM-MVS GCP configurations.

Table 3
Percentage contribution of rockfall size fractions to overall eroded volume for TLS- and SfM-based change detection.

Rockfall volume (m^3)	% contribution to total rockfall volume				
	TLS	GCP_{sp}	GCP_{mod}	GCP_{den}	GCP_{ex}
0.001–0.01	3.75	2.05	3.62	4.19	3.29
0.01–0.1	6.96	6.00	9.11	9.59	8.69
0.1–1	11.64	4.75	7.86	9.04	12.11
1–10	42.45	28.66	34.64	24.06	33.38
>10	35.21	58.55	44.76	53.12	42.54

differences in TLS and SfM data density and spatial coverage, particularly in partly occluded areas, can produce differences in the position of the reconstructed surface. Data quality issues associated with TLS viewshed could be overcome by occupying more station positions along the foreshore to improve coverage and provide additional data overlap between successive stations. However, in our case, and many others, site-specific constraints such as foreshore complexity, the inaccessibility of optimal scanning positions, and tidal activity hinders this approach.

The differencing of repeat SfM-MVS datasets has yielded data describing patterns and rates of coastal erosion that are comparable with those retrieved via repeat TLS. Our initial analysis revealed that high magnitude but low frequency rock falls account for a disproportionately large fraction of the total eroded volume. Specifically, failures $<0.07\ m^3$ account for <3% of the total eroded volume for both SfM and TLS results, implying that smaller volume failures are a less important constituent of cliff face recession in this setting. In contrast, larger episodic failures can produce locally elevated rates of cliff line retreat (e.g. >0.5 m per event), which can exceed the mean by over an order of magnitude, and are likely to be of more concern to coastal managers.

In light of the volumetric inconsistencies between intersecting SfM- and TLS-detected rock falls (Fig. 9), we find it is necessary to implement an additional size threshold filter to remove rock falls $<0.07\ m^3$. In this way, we adapt the approach of filtering raw surface change using a standard level of detection, which generally reflects the combined survey error and which is employed in the first instance as the primary method for removing artificial change resulting from model-to-model alignment error (e.g. (Lim et al., 2005; Rosser et al., 2013; Vann Jones et al., 2015)). Our volumetric filtering removes >74% of instances of surface change but has a negligible effect on spatially averaged rates of cliff face retreat. However, we emphasis the caveat that, whilst this volumetric threshold appears to be suitable for our study site, it should be applied to other sites with caution.

We assume throughout that the results of TLS differencing are an accurate and reliable benchmark against which to compare the number and volume of detected rock falls. If this is indeed the case, it follows that the additional rock falls which are detected as the result of GCP network densification may not be genuine, and might be the product of the propagation of 3D surface deformations, which, when differenced, are manifested as cliff surface erosion. Conversely, if we assume that the SfM-derived rockfall inventories provide a more accurate representation of reality, it follows that overall total eroded volumes (and erosion rates) could be up to 38% higher than those derived from TLS differencing (Fig. 7a).

However, two unresolved questions remain, namely the attribution of volumetric inconsistencies between SfM- and TLS-derived rock falls $<0.07\ m^3$ (Fig. 9) and to what extent these inconsistencies are the result of data errors associated with either technology. Our emphasis has been on establishing a level of detection whereby TLS- and SfM-derived rock fall volumes are comparable and which could be applied in other coastal cliff environments. For the smallest rock falls, it becomes difficult to qualitatively, or quantitatively, establish whether individual rock falls are genuine in either dataset, or are data errors. As such, we are confident that above $>0.07\ m^3$ both the TLS and SfM rockfall inventories are an accurate reflection of reality, whilst our confidence in the accuracy of smaller rockfalls is lower. Since we identify numerous small rockfalls that intersect their counterparts in each dataset, we are convinced that these are indeed genuine events, but more work is required to establish which differencing dataset generates the most realistic volumes. Specifically, further work should attempt to isolate the reason(s) for this clearly identifiable volumetric threshold, thereby making it more straightforward to establish and apply a similar method at other sites where a control dataset does not exist. As such, the application of our specific threshold to rock fall inventories from other sites should be considered with caution. Future work might explore might include the use high-resolution SfM input photography or orthophotography as a means with which to verify or discard rock fall events based on a comparison of pre- and post-event cliff visual texture or appearance. Elsewhere, full 3D 'cloud-to-cloud' differencing techniques have been shown to perform favourably for reliably reducing threshold levels of change detection across complex cliff terrain using repeat TLS surveys (e.g. (Lague et al., 2013; Williams et al., 2017)). Further work is required to explore whether these improvements in the level of detection are equally applicable to SfM-derived surface models, and, crucially, whether such methods are accessible to practitioners.

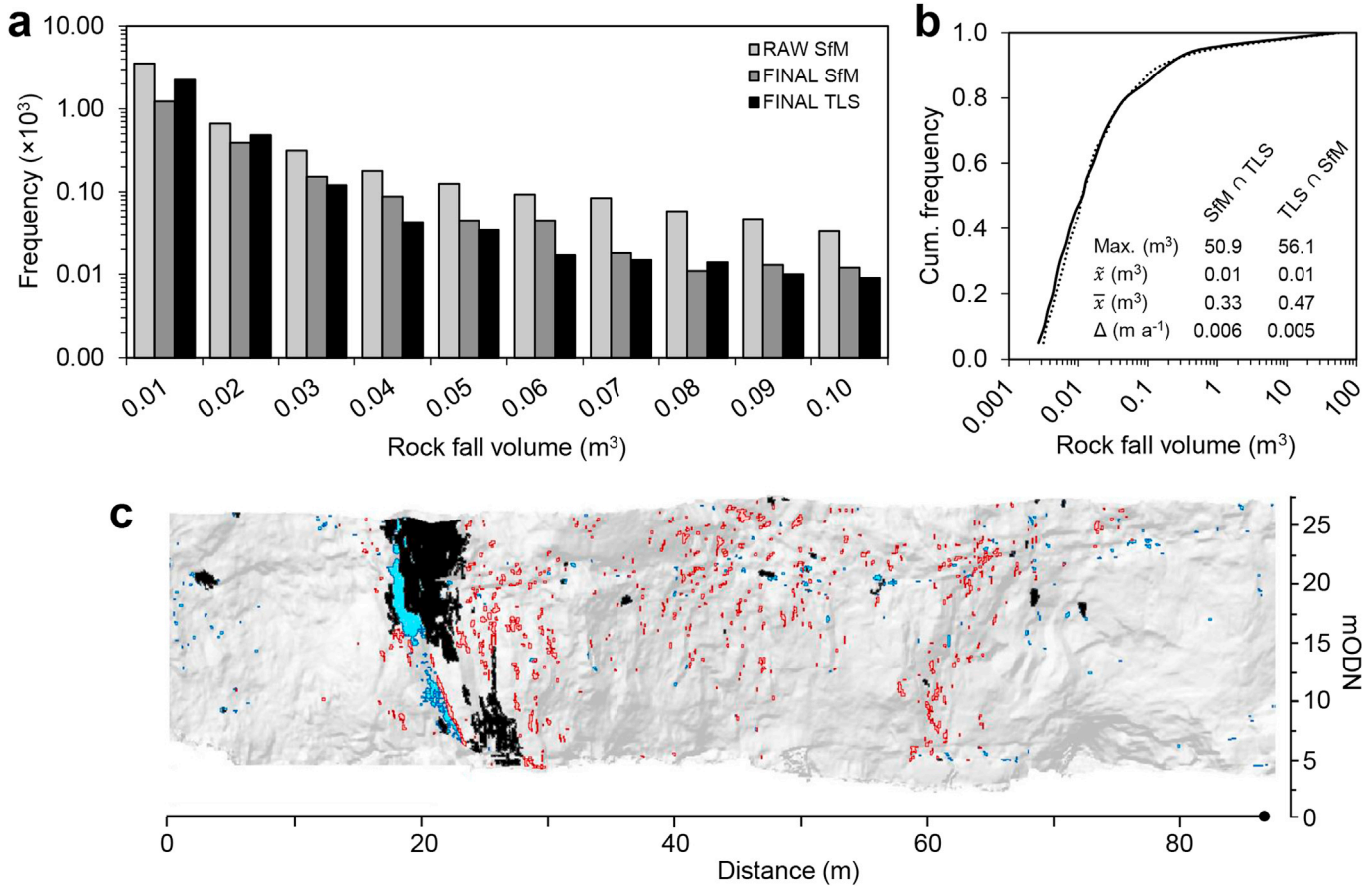

Fig. 8. Refinement of rock fall volumetric statistics. a) Refinement of rock fall frequency data for incremental 0.01 m^3 bins following post-processing. b) Cumulative frequency data for intersecting rock falls. Solid black = SfM rock falls, dashes = TLS rock falls. Summary statistics also shown for intersecting data, including median ($\tilde{x}$) and mean ($\bar{x}$) rock fall volume, and calculated erosion rate over the wider study area(Δ). c) visualisation of SfM-detected rock falls following initial thresholding and filtering (red), and SfM-detected rock falls that intersect the equivalent TLS-derived rock falls (black). Filtered (non-intersecting) TLS-derived rock falls are shown in blue. See Fig. 1 for location. (For interpretation of the references to colour in this figure legend, the reader is referred to the Web version of this article.)

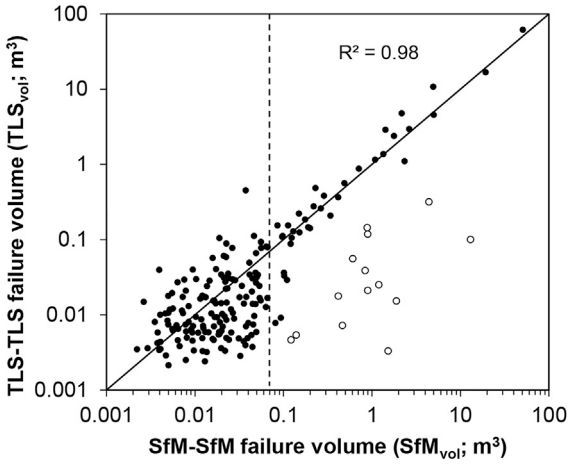

Fig. 9. Relationship between discrete intersecting TLS-TLS and SfM-SfM eroded volumes (GCP_{mod}). Vertical dashed line indicates the 0.07 m^3 SfM-SfM cutoff which was implemented to refine overall eroded volume and erosion rate. White data points identify rock falls >0.07 m^3 which are not completely reconstructed by the TLS data due to topographic occlusion. R^2 value applies to data >0.07 m^3.

Following volumetric thresholding, the mean rate of retreat and mean rock fall volume across the site, as established using both technologies, is in line with the results from existing high-resolution erosion monitoring studies along the UK North Sea coast (e.g. (Lim et al., 2005; Lim et al., 2010; Rosser et al., 2013)). Mean rates of cliff face retreat differ by 0.001 m a^{-1} across the ~1 km study area, which we deem negligible for operational implementation. For example, over a 100-year forecasting period, mean retreat rates generated from TLS or SfM-MVS differencing would diverge by up to 0.1 m (SfM-MVS erosion monitoring would produce a 0.7 m landward recession, while TLS would produce a loss of 0.6 m). Of more practical relevance is the ability of SfM-MVS derived face differencing to accurately reconstruct large failures, which are also detected by TLS differencing.

4.2. *Terrestrial SfM-MVS: an effective, accessible and responsive tool for coastal practitioners*

The increasing availability, consistency and capability of TLS systems have made them the industry standard for quantifying the erosion of coastal cliffs at high spatial resolution and accuracy. This specialised approach requires skilled operation, processing and interpretation and is not logistically suited to covering extensive (>1 km-long) cliff sections, although the increasing range (>1 km), affordability and portability of TLS systems have begun to address this limitation. TLS application to erosion monitoring remains constrained by purchase cost and a requirement to deploy the system, often at multiple station positions, in front of the cliff face for the duration of data collection (usually in the order of 30 min or more at each station). The finance, skilled personnel and sufficiently large low tide conditions required to collect TLS data on the cliff surface mean that surveys are often infrequent and are

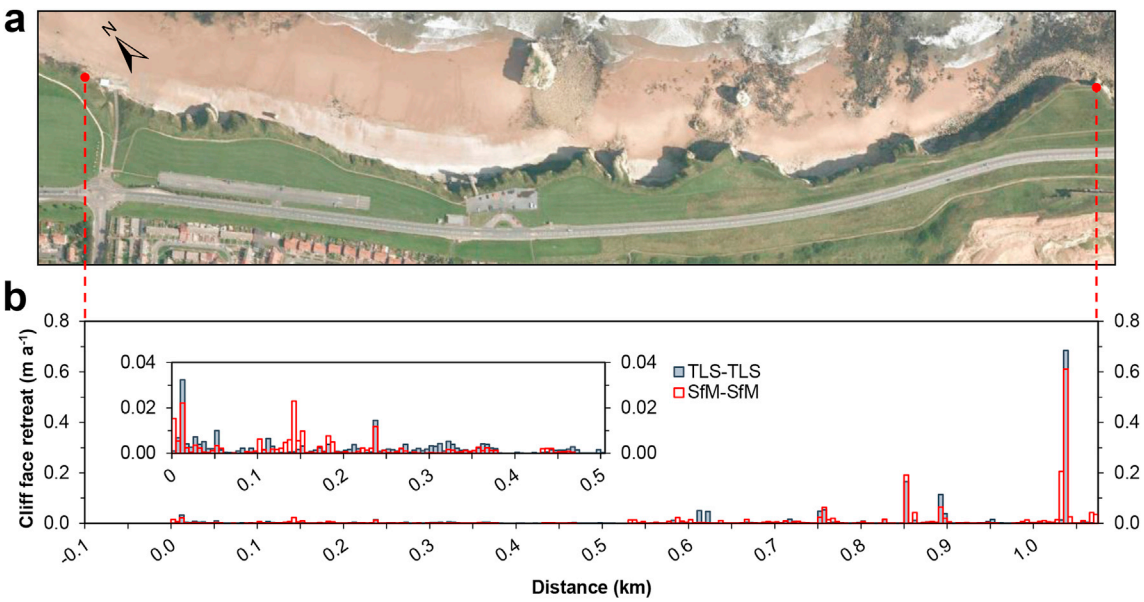

Fig. 10. Cliff face retreat at Marsden Bay. a) context map. b) annual face retreat calculated from TLS (solid grey) and SfM (hollow red) differencing and displayed as total retreat within 5 m cliff length bins. Inset panel shows rescaled data from 0 to 0.5 km. Red dashes show start and end point of the monitored area. (For interpretation of the references to colour in this figure legend, the reader is referred to the Web version of this article.)

particularly limited with respect to responsive surveys following failure events. Therefore, key data on the nature and extent of the failure and the likelihood of progressive slope instability are rarely available to managers and decision makers.

Here we have demonstrated the potential of terrestrial SfM-MVS methods for efficiently generating kilometre-scale, spatially distributed erosion metrics for a section of hard rock coastal cliffs. Terrestrial SfM-MVS methods represent a demonstrable improvement on existing approaches through quantifiable gains in field deployment time whilst reducing purchase and logistical costs. Critically, such data can be easily acquired using a consumer-grade, compact digital camera, or even a smartphone (Micheletti et al., 2014), and are relatively straightforward to acquire by a coastal manager or engineer who is familiar with the approach. At certain sites which experience significant public footfall, this idea could be further developed to incorporate opportunistic 'crowdsourcing' of SfM-MVS input photographs to extend datasets and effect participatory involvement from members of the public (e.g. (Frahm et al., 2013; Snavely et al., 2008; Sofia et al., 2016)). Whilst 3D model generation and analysis require specialist software knowledge and experience in 3D data manipulation and presentation, responsive and wide-scale primary data capture is accessible to coastal practitioners for the first time.

Our findings have implications for aspects of coastal monitoring, planning and civil engineering. Our results closely mirror those retrieved using TLS, and support the use of terrestrial SfM-MVS methods as a viable alternative to existing methods of coastal erosion monitoring. Planners or civil engineers operating in the coastal zone have the option of undertaking or commissioning bespoke and financially viable terrestrial SfM-guided erosion monitoring programmes to augment coastal management or engineering projects at the development, implementation or construction, and project evaluation stages. For example, such methods would be appropriate for quantifying baseline erosion rates of a coastal cliff prior to the design of a wave defence structure at the cliff toe, or the implementation of cliff stabilisation works. Repeat SfM surveys could then be used to benchmark pre-construction 3D cliff face change and erosion rates against those observed post-construction, ideally as part of a longer-term erosion monitoring programme.

The analysis of 3D change detection data for coastal cliffs can provide valuable insights into the spatial and temporal distribution of coastal response to environmental or anthropogenic forcing and thereby facilitate targeted management. Currently, coastal management decisions can be based on a single rate of cliff retreat that is deemed to be representative of extensive (tens of kilometres) and often complex sections of coastline where local erosion rates may in fact vary by an order of magnitude or more (e.g. (Lim et al., 2005; Moore and Griggs, 2002)). Such simplifications, whilst necessary to date, are insufficient for accurately characterising the variable erosion response of coastal cliffs, and responding to these accordingly. For example, repeat terrestrial SfM-MVS methods are highly suited for rapid anticipatory deployment to identify pre-cursory behaviour prior to a large failure event (e.g. (Rosser et al., 2007)) and can be deployed in a responsive manner to quantify the response and adjustment of sections of coastline following storm activity (e.g. (Turner et al., 2016)).

5. Conclusions

Emergent SfM-MVS methods represent a low-cost and accurate method for reconstructing coastal topography at spatial and temporal resolutions that permit the identification of individual rock falls and the extraction of erosion rates comparable to those derived from TLS. Such approaches represent a viable monitoring solution for coastal practitioners, who can collect input data rapidly and responsively without significant specialist training and at low cost. This study has demonstrated the capability of repeat terrestrial SfM-MVS for quantifying erosion of a ~1 km section of rock cliff face along the north-east coast of the UK. Our main findings and recommendations are summarised as follows:

- SfM-MVS input photosets of coastal cliff faces can be acquired by non-specialists using a consumer-grade digital cameras.
- Locating survey control points along the cliff top and base at a horizontal spacing which approximates the cliff height balances user interaction and model refinement with acceptable accuracies relative to equivalent TLS data.
- Correspondence between intersecting TLS- and SfM-detected rock fall volumes improves beyond a 0.07 m^3 volumetric threshold. This threshold is used to refine SfM-MVS erosion data.
- At the kilometre scale, TLS and SfM derived erosion rates are comparable (0.6×10^{-2} m a^{-1} and 0.7×10^{-2} m a^{-1}) and are in line with regional observations, yet are lower than existing local predictions of

coastal retreat, which are ~0.2 m a^{-1}. Patterns of retreat are spatially variable, and can locally exceed the background erosion rate by over an order of magnitude.

- To fully realise the value of high spatial and temporal resolution erosion data to coastal engineers and managers, consideration should be given as to how this information could be effectively incorporated into existing monitoring and management frameworks.

Acknowledgements

This research was funded by and conducted in collaboration with South Tyneside Council (grant reference NOS302C/000A/013A) who we gratefully acknowledge. Bradley Sparkes, Tom Winstanley, Thomas Shaw and Stuart Dunning are thanked for their assistance with field data collection. We additionally acknowledge the support of the Northumbria University Virtual Reality and Visualisation Group. North Shields tidal data were downloaded from the British Oceanographic Data Centre (www.bodc.ac.uk).

Appendix A. Supplementary data

Supplementary data related to this article can be found at https://doi.org/10.1016/j.coastaleng.2018.04.008.

References

Abellán, A., Oppikofer, T., Jaboyedoff, M., Rosser, N.J., Lim, M., Lato, M.J., 2014. Terrestrial laser scanning of rock slope instabilities. Earth Surf. Process. Landforms 39, 80–97.

Agisoft, 2016. Agisoft PhotoScan User Manual: Professional Edition, V. 1.2.6. Agisoft.

Baily, B., Nowell, D., 1996. Techniques for monitoring coastal change: a review and case study. Ocean Coast Manag. 32 (2), 85–95.

Baptista, P., Cunha, T., Bernardes, C., Gama, C., Ferreira, Ó., 2011. A. Dias, A precise and efficient methodology to analyse the shoreline displacement rate. J. Coast Res. 27 (2), 223–232.

Bray, M.J., Hooke, J.M., 1997. Prediction of soft-cliff retreat with accelerating sea-level rise. J. Coast Res. 13 (2), 453–467.

Brooks, S.M., Spencer, T., 2010. Temporal and spatial variations in recession rates and sediment release from soft rock cliffs, Suffolk coast, UK. Geomorphology 124, 26–41.

Brunier, G., Fleury, J., Anthony, E.J., Gardel, A., Dussouillez, P., 2016. Close-range Structure-from-Motion photogrammetry from high-resolution beach morphometric surveys: examples from an embayed rotating beach. Geomorphology 261, 76–88.

Bruun, P., 1962. sea-level rise as a cause of shore erosion, proceedings of the american society of civil engineers. J. Waterw. Harb. Div. 88, 117–130.

Carbonneau, P.E., Dietrich, J.T., 2016. Cost-effective non-metric photogrammetry from consumer-grade sUAS: implications for direct georeferencing of structure from motion photogrammetry. In: Earth Surface Processes and Landform.

Carrivick, J.L., Smith, M.W., Quincey, D.J., 2016. Structure from Motion in the Geosciences. Wiley-Blackwell, London.

Casella, E., Rovere, A., Pedronicini, A., Startk, C.P., Casella, M., Ferrari, M., Firpo, M., 2016. Drones as tools for monitoring beach topography changes in the Ligurian Sea (NW Mediterranean). Geo Mar. Lett. 36 (2), 151–163.

Collins, B.D., Sitar, N., 2008. Processes of coastal bluff erosion in weakly lithified sands, Pacifica, California, USA. Geomorphology 97, 483–501.

Cooper, J.A.G., Pilkey, O.H., 2004. Sea-level rise and shoreline retreat: time to abandon the Bruun Rule. Global Planet. Change 43, 157–171.

Costa, S., Delahaye, D., Freiré-Diaz, S., Di Nocera, L., Davidson, R., Plessis, E., 2004. Quantification of the Normany and Picardy chalk cliff retreat by photogrammetric analysis. Eng. Geol. Spec. Publ. 20, 139–148.

Davidson-Arnott, R.G.D., 2005. Conceptual model of the effects of sea level rise on sandy coasts. J. Coast Res. 21 (6), 1166–1172.

Dawson, R.J., Dickson, M.E., Nicholls, R.J., Hall, J.W., Walkden, M.J.A., Stansby, P.K., Mokrech, M., Richards, J., Zhou, J., Milligan, J., Jordan, A., Pearson, S., Rees, J., Bates, P.D., Koukoulas, S., Watkinson, A.R., 2009. Integrated analysis of risks of coastal flooding and cliff erosion under scenarios of long term change. Climatic Change 95, 249–288.

Dewez, T.J.B., 2004. Reconstructing 3D coastal cliffs from airborne oblique photographs without ground control points, ISPRS Annals of the Photogrammetry. Rem. Sens. Spatial Inf. Sci. II (5), 4 pp.

Dewez, T.J.B., Rohmer, J., Regard, V., Cnudde, C., 2013. Probabilistic coastal cliff collapse hazard from repeated terrestrial laser surveys: case from Mesnil Val (Normandy, northern France). J. Coast Res. 65, 702–707. Special Issue.

Dewez, T.J.B., Leroux, J., Morelli, S., 2016. Cliff collapse hazard from repeated multicopter UAV acquisitions: return on experience, ISPRS Annals of the Photogrammetry. Rem. Sens. Spatial Inf. Sci. II (5), 7pp.

Dickson, M.E., Walkden, M.J.A., Hall, J.W., 2007. Systematic impacts of climate change on an eroding coastal region over the twenty-first century. Climatic Change 84, 141–166. https://doi.org/10.1007/s10584-006-9200-9.

Dornbusch, W., Robinson, D.A., Moses, C.A., Williams, R.B.G., 2008. Temporal and spatial variations of chalk cliff retreat in East Sussex, 1873-2001. Geomorphology 249, 271–282.

Drummond, C.D., Harley, M.D., Turner, I.L., Matheen, A.N.A., Glamore, W.C., 2015. UAV Applications to Coastal Engineering. In: Australasian Coasts and Ports Conference 2015, 15–18 September. Auckland, New Zealand, 6 pp.

Earlie, C.S., Masselink, G., Russell, P.E., Shail, R.K., 2015. Application of airborne LiDAR to investigate rates of recession in rocky coast environments. J. Coast Conserv. 19 (6), 831–845.

Environment Agency, 2009. Shoreline management plans (SMPs). Flooding and coastal change policy paper. Available. https://www.gov.uk/government/publications/shoreline-management-plans-smps.

European Commission, 2006. Towards a future Maritime Policy for the Union: a European vision for the oceans and seas. In: Commission of the European Communities Green Paper, COM, p. 275. Available. http://europa.eu/documents/comm/green_papers/pdf/com_2006_0275_en_part2.pdf.

Feagin, R.A., Williams, A.M., Popescu, S., Stukey, J., Washington-Allen, R.A., 2014. The use of terrestrial laser scanning (TLS) in dune ecosystems: the lessons learned. J. Coast Res. 30 (1), 111–119.

Frahm, J.-M., Heinly, J., Zheng, E., Dunn, E., Fite-Georgel, P., Pollefeys, M., 2013. Geo-registered 3D models from crowdsourced image collections. Geo-spatial Info. Sci. 16 (1), 55–60.

Genz, A.S., Fletcher, C.H., Dunn, R.A., Frazer, L.N., Rooney, J.J., 2007. The predictive accuracy of shoreline change rate methods and alongshore beach variation on Maui, Hawaii. J. Coast Res. 23 (1), 87–105.

Gibbs, A.E., Nolan, M., Richmond, B., 2015. Evaluating changes to Arctic coastal bluffs using repeat aerial photography and structure-from-motion elevation models. In: Wang, P., Rosati, J.D., Cheng, J. (Eds.), Coastal Sediments 2015: the Proceedings of the Coastal Sediments. World Scientific.

Gienko, G.A., Terry, J.P., 2014. Three-dimensional modeling of coastal boulders using multi-view image measurements. Earth Surf. Process. Landforms 39, 853–864.

Gonçalves, J.A., Henriques, R., 2015. UAV photogrammetry for topographic monitoring of coastal areas. ISPRS J. Photogrammetry Remote Sens. 104, 101–111.

Gulyaev, S.A., Buckeridge, J.S., 2004. Terrestrial methods for monitoring cliff erosion in an urban environment. J. Coast Res. 20 (3), 871–878.

Hall, J.W., Dawson, R.J., Sayers, P.B., Rosu, C., Chatterton, J.B., Deakin, R., 2003. A methodology for national-scale flood risk assessment. Water Marit. Eng. 156, 235–247.

Harwin, S., Lucieer, A., 2012. Assessing the accuracy of georeferenced point clouds produced via multi-view stereopsis from unmanned aerial vehicle (UAV) imagery. Rem. Sens. 4, 1573–1599.

James, M.R., Robson, S., 2012. Straightforward reconstruction of 3D surfaces and topography with a camera: accuracy and geoscience application. J. Geophys. Res. 117. F03017.

James, M.R., Robson, S., 2014. Mitigating systematic error in topographic models derived from UAV and ground-based image network. Earth Surf. Process. Landforms 39, 1413–1420.

James, M.R., Robson, S., d'Oleire-Oltmanns, S., Niethammer, U., 2017. Optimising UAV topographic surveys processed with structure-from-motion: ground control quality, quantity and bundle adjustment. Geomorphology 280, 51–66.

James, M.R., Robson, S., Smith, M.W., 2017. 3-D uncertainty-based topographic change detection with structure-from-motion photogrammetry: precision maps for ground control and directly georeferenced surveys. Earth Surf. Process. Landforms 42, 1769–1788.

Kuhn, D., Prüfer, S., 2014. Coastal cliff monitoring and analysis of mass wasting processes with the application of terrestrial laser scanning: a case study of Rügen, Germany. Geomorphology 213, 153–165.

Lague, D., Brodu, N., Leroux, J., 2013. Accurate 3D comparison of complex topography with terrestrial laser scanner: application to Rangitikei canyon (NZ). ISPRS J. Photogrammetry Remote Sens. 82, 10–26.

Lazarus, E.D., Ellison, M.A., Murray, A.B., Hall, D.M., 2016. An evolving research agenda for human-coastal systems. Geomorphology 256, 81–90.

Letortu, P., Costa, P., Maquaire, O., Delacourt, C., Augereau, E., Davidson, R., Suanez, S., Nabucet, J., 2015. Retreat rates, modalities and agents responsible for erosion along the coastal chalk cliffs of Upper Normandy: the contribution of terrestrial laser scanning. Geomorphology 245, 3–14.

Lim, M., Petley, D.N., Rosser, N.J., Allison, R.J., Long, A.J., Pybus, D., 2005. Combined digital photogrammetry and time-of-flight laser scanning for monitoring cliff evolution. Photogramm. Rec. 20, 109–129.

Lim, M., Rosser, N.J., Allison, R.J., Petley, D.N., 2010. Erosional processes in the hard rock cliffs at Staithes, North Yorkshire. Geomorphology 114, 12–21.

Lim, M., Dunning, S.A., Burke, M., King, H., King, N., 2015. Quantification and implications of change in organic carbon bearing coastal dune cliffs: a multiscale analysis from the Northumberland coast, UK. Remote Sens. Environ. 163, 1–12.

Loos, E.A., Niemann, K.O., 2002. Shoreline feature extraction from remotely-sensed imagery. Geosci. Rem. Sens.IGARSS IEEE Int 6, 3417–3419.

Maiti, S., Bhattacharya, A.K., 2009. Shoreline change analysis and its application to prediction: a remote sensing and statistics based approach. Mar. Geol. 257, 11–23.

Mancini, F., Dubbini, M., Gattelli, M., Stecchi, F., Fabbri, S., Gabbianelli, G., 2013. Using unmanned aerial vehicles (UAV) for high-resolution reconstruction of topography: the Structure-from-Motion approach on coastal environments. Rem. Sens. 5 (12), 6880–6898.

Micheletti, N., Chandler, J.H., Lane, S.N., 2014. Investigating the geomorphological potential of freely available and accessible structure-from-motion photogrammetry using a smartphone. Earth Surf. Process. Landforms 40 (4), 473–486.

Mills, J.P., Buckley, S.J., Mitchell, H.L., Clarke, P.J., Edwards, S.J., 2005. A geomatics data integration technique for coastal change monitoring. Earth Surf. Process. Landforms 30 (6), 651–664.
Montreuil, A.-L., Bullard, J., Chandler, J., 2013. Detecting seasonal variations in embryo dune morphology using a terrestrial laser scanner. J. Coast Res. 65 (2), 1313–1318. Special Issue.
Moore, L.J., 2000. Shoreline mapping techniques. J. Coast Res. 16 (1), 111–124.
Moore, L.J., Griggs, G.B., 2002. Long-term cliff retreat and erosion hotspots along the central shores of the monterey bay national marine sanctuary. Mar. Geol. 181, 265–283.
Mulder, J.P.M., Hommes, S., Horstman, E.M., 2011. Implementation of coastal erosion management in The Netherlands. Ocean Coast Manag. 54, 888–897.
Nicholls, R.J., Townend, I.H., 2013. A.P.Bradbury, D. Ramsbottom, S.A. Day, planning for long-term coastal change: experiences from England and Wales. Ocean Eng. 71, 3–16.
Obu, J., Lantuit, H., Grosse, G., Günther, F., Sachs, T., Helm, V., Fritz, M., 2017. Coastal erosion and mass wasting along the Canadian Beaufort Sea based on annual airborne LiDAR elevation data. Geomorphology 293B, 331–346.
Oyedotun, T.D.T., 2014. Shoreline Geometry: DSAS as a Tool for Historical Trend Analysis. *Geomorphological Techniques*, Chapter 3, Section 2.2. British Society for Geomorphology online publication. Available. http://www.geomorphology.org.uk/geomorph_techniques.
Palaseanu-Lovejoy, M., Danielson, J., Thatcher, C., Foxgrover, A., Barnard, P., Brock, J., Young, A., 2016. Automatic delineation of seacliff limits using Lidar-derived high-resolutions DEMs in Southern California. J. Coast Res. 76, 162–173. Special Issue.
Pardo-Pascual, J.E., Amonacid-Caballer, J., Ruiz, L.A., Palomar-Vázquez, J., 2012. Automatic extraction of shorelines from Landsat TM and ETM+ multi-temporal images with subpixel precision. Remote Sens. Environ. 123, 1–11.
Penning-Rowsell, E.C., Pardoe, J., 2015. The distributional consequences of future flood risk management in England and Wales. Environ. Plann. C Govern. Pol. 33, 1301–1321.
Pethick, J., 2001. Coastal management and sea-level rise. Catena 42, 307–322.
Pierre, G., 2006. Processes and rate of retreat of the clay and sandstone sea cliffs of the northern Boulonnais (France). Geomorphology 73, 64–77.
Pranzini, E., Wetzel, L., Williams, A.T., 2015. Aspects of coastal erosion and protection in Europe. J. Coast Conserv. 19, 445–459.
Pye, K., Blott, S.J., 2016. Assessment of beach and dune erosion and accretion using LiDAR: impact of the stormy 2013-14 winter and longer term trends on the Sefton Coast, UK. Geomorphology 266, 146–167.
Roebeling, P.C., Costa, L., Magalhães-Filho, L., Tekken, V., 2013. Ecosystem service value losses from coastal erosion in Europe: historical trends and future projections. J. Coast Conserv. 17, 389–395.
Rosser, N.J., Petley, D.N., Lim, M., Dunning, S.A., Allison, R.J., 2005. Terrestrial laser scanning for monitoring the process of hard rock coastal cliff erosion. Q. J. Eng. Geol. Hydrogeol. 38, 363–375.
Rosser, N.J., Lim, M., Petley, D.N., Dunning, S.A., Allison, R.J., 2007. Patterns of precursory rock fall prior to slope failure. J. Geophys. Res.: Earth Surface 112. F04014.
Rosser, N.J., Brain, M.J., Petley, D.N., Lim, M., Norman, E.C., 2013. Coastline retreat via progressive failure of rocky coastal cliffs. Geology 41 (8), 939–942.
Ružić, I., Marović, I., Benac, C., Ilić, S., 2014. Coastal cliff geometry derived from structure-from-motion photogrammetry at Stara Baška, Krk Island, Croatia. Geo Mar. Lett. 34, 555–565.
Sear, D.A., Bacon, S.R., Murdock, A., Doneghan, G., Baggaley, P., Serra, C., LeBas, T.P., 2011. Cartographic, geophysical and diver surveys of the Medieval town site at Dunwich, Suffolk, England. Int. J. Naut. Archaeol. 40 (1), 113–132.
Smith, M.W., Carrivick, J.L., Quincey, D.J., 2015. Structure from motion photogrammetry in physical geography. Prog. Phys. Geogr. 40 (2), 247–275.
Snavely, N., Seitz, S.N., Szeliski, R., 2008. Modeling the world from photo collections. Int. J. Comput. Vis. 80, 189–210.
Sofia, G., Masin, R., Tarolli, P., 2016. Prospects for crowdsourced information on the geomorphic 'engineering' by the invasive Coypu (*Myocastor coypus*). Earth Surf. Process. Landforms 42, 365–377.
Thieler, E.R., Danforth, W.W., 1994. Historical shoreline mapping (I): improving techniques and reducing positioning errors. J. Coast Res. 10 (3), 549–563.
Thieler, E.R., Danforth, W.W., 1994. Historical shoreline mapping (ii): application of the digital shoreline mapping and analysis systems (DSMS/DSAS) to shoreline change mapping in Puerto Rico. J. Coast Res. 10 (3), 600–620.
Turner, I.L., Harley, M.D., Drummond, C.D., 2016. UAVs for coastal surveying. Coast Eng. 114, 19–24.
Vann Jones, E.C., Rosser, N.J., Brain, M.J., Petley, D.N., 2015. Quantifying the environmental controls on erosion of a hard rock cliff. Mar. Geol. 363, 230–242.
Warrick, J.A., Ritches, A.C., Adelman, G., Adelman, K., Limber, P.W., 2017. New techniques to measure cliff change from historical oblique aerial photographs and Structure-from-Motion photogrammetry. J. Coast Res 33 (1), 39–55.
Westoby, M.J., Brasington, J., Glasser, N.F., Hambrey, M.J., Reynolds, J.M., 2012. 'Structure-from-Motion' photogrammetry: a low-cost, effective tool for geoscience applications. Geomorphology 179, 300–314.
White, K., El Asmar, H.M., 1999. Monitoring changing position of coastlines using Thematic Mapper imagery, an example from the Nile Delta. Geomorphology 29 (1–2), 93–105.
Williams, R., 2012. DEMs of difference. In: Cook, S.J., Clarke, L.E., Nield, J.M. (Eds.), Geomorphological Techniques. British Society for Geomorphology, London chapter 2(3.2), online. http://www.geomorphology.ord.uk/geomorph_techniques.
Williams, J.G., Rosser, N.J., Hardy, R.J., Brain, M.J., Afana, A.A., 2017. Optimising 4D approaches to surface change detection: improving understanding of rockfall magnitude-frequency. In: Earth Surface Dynamics Discussions. https://doi.org/10.5194/esurf-2017-43.
Young, A.P., Guza, R.T., O'Reilly, W.C., Flick, R.E., Gutierrez, R., 2011. Short-term retreat statistics of a slowly eroding coastal cliff. Nat. Hazards Earth Syst. Sci. 11, 205–217.